# Acoustic band gaps of three-dimensional periodic polymer cellular solids with cubic symmetry

Cite as: J. Appl. Phys. **114**, 043521 (2013); https://doi.org/10.1063/1.4817168
Submitted: 12 June 2013 . Accepted: 09 July 2013 . Published Online: 31 July 2013

Yanyu Chen, Haimin Yao, and Lifeng Wang

# Acoustic band gaps of three-dimensional periodic polymer cellular solids with cubic symmetry

Yanyu Chen,[1] Haimin Yao,[2] and Lifeng Wang[1,3,a)]
[1]*Department of Civil and Environmental Engineering, Clarkson University, Potsdam, New York 13699, USA*
[2]*Department of Mechanical Engineering, The Hong Kong Polytechnic University, Hung Hom, Kowloon, Hong Kong*
[3]*Department of Mechanical Engineering, Stony Brook University, Stony Brook, New York 11790, USA*

(Received 12 June 2013; accepted 9 July 2013; published online 31 July 2013)

The band structure and sound attenuation of the triply periodic co-continuous composite materials with simple cubic lattice, body-centered cubic lattice, and face-centered cubic lattice consisting of PMMA and air are investigated using finite element method. Complete band gaps are found in these structures and the width of band gaps is depending on volume fraction. It is shown that the width of band gaps along different directions in the first irreducible Brillouin zone enlarges as the volume fraction increases from 0.2 to 0.7. The largest complete band gap widths of the three types of co-continuous structures are 0.29, 0.54, and 0.55, respectively. As the complete band gaps appear in audible range of frequencies, these triply periodic co-continuous composite materials can be utilized to control noise. © *2013 AIP Publishing LLC*. [http://dx.doi.org/10.1063/1.4817168]

## I. INTRODUCTION

The propagation of acoustic and elastic waves in periodic composite materials has attracted a great deal of research interest in recent years. Periodic composite materials, exhibiting complete band gaps (CBGs) in which the acoustic waves and elastic waves cannot propagate along any direction, are called phononic crystals. The underlying mechanism lies in the multiple scattering of a mechanical wave at the interfaces between materials with different mechanical properties. Therefore, phononic crystals have many exciting applications such as sound filters,[1] noise control,[2] acoustic wave guides,[3] Anderson localization,[4] acoustic mirage,[5] vibration control for high-precision mechanical system,[6] shock wave propagation in body armor,[7,8] as well as the seismic wave, and ocean wave propagation in civil engineering.[9–12]

One motivation of the study is to find large complete band gaps in 3D cellular solids. In the past two decades, theoretical and experimental investigations have been conducted on band structures and transmission/attenuation of periodic structures. Kushwaha *et al*. have theoretically investigated the band structures of 2D square and hexagonal lattices and 3D cubic lattices, which are consisted of solid-solid, liquid-liquid, and solid-liquid system by plane wave expansion method (PWE). The influences of the geometry and material properties on the width of band gaps have been discussed.[13–16] Economou and Sigalas[17] and Garcia-Pablos *et al*.[18] have studied the complete band gaps of elastic wave in periodic composite materials by PWE and finite difference time domain method (FDTD), respectively, and concluded that the lattice structure, shape of inclusion, size and contrast of material properties are vital to the formation of CBG. The influence of geometry and material properties of the composite materials has also been reported by Goffaux and Vigneron[19] and Vasseur *et al*.,[20] respectively. Montero *et al*. have experimentally observed complete band gap in 2D composite materials and found reasonable agreement with theoretical predications.[21] Vasseur *et al*. have also experimentally supported the existence of acoustic complete band gaps predicted by PWE and FDTD in 2D periodic composite materials.[20] More recently, Cui *et al*. and Wu and Chen have employed finite element method (FEM) to calculate the band structure of steel tubes and polymethyl methacrylate (PMMA) in air, respectively, and they have also compared the simulated and experimental measured data and found good agreement.[22,23] A more comprehensive progress on theoretical and experimental investigation on phononic crystal is reported by Sigalas *et al*. in their review paper.[24]

However, most of these studies are from the pure physical perspective, for example, some of the structures are not self-supported and some cannot be fabricated easily in practice. This limits their potential application in engineering even though these composite structures exhibit large CBGs. It is still a challenge to design and fabricate 3D periodic composite structures with desired CBGs and well-defined topology.

Recently, triply periodic minimal surfaces have been of great interest to mathematicians, physical scientists, material scientists, and biologists. Minimal surfaces and triply periodic structures arise in a variety of systems, such as block copolymers,[25] nano-composites,[26] and biological exoskeletons.[27] Prior works have found these structures exhibit enhanced elastic properties compared to their rod-connected model counterparts[28] and they are also ideal for multifunctional optimization, such as simultaneous transport of heat and electricity and enhanced bulk modulus and conductivity.[29,30] Moreover, these co-continuous structures can be fabricated at different length scale, such as by interference lithography for sub-micrometer length scale structures[28] and 3-D printing for millimeter length scale structures.[31] Herein, we study the acoustic wave propagation in these structures to enhance their multifunctionality.

a)Electronic mail: lifwang@clarkson.edu

 

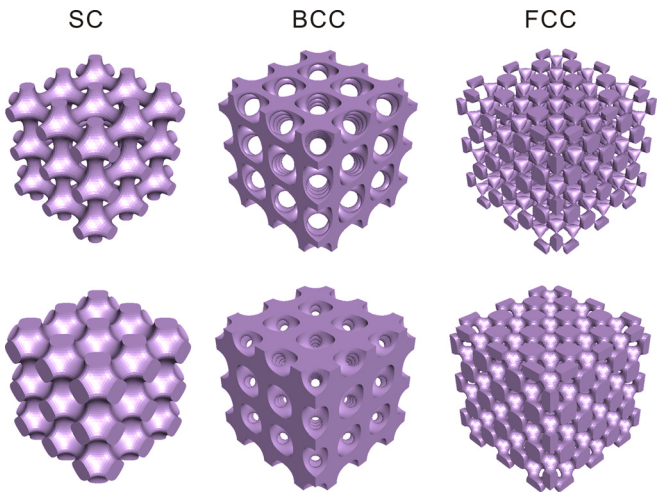


FIG. 1. 3D periodic microstructures consisting of $3 \times 3 \times 3$ unit cells with SC, BCC, and FCC lattices and two volume fractions are shown (~25% and 50%).

In this paper, we consider co-continuous structures with simple cubic (SC), body-centered-cubic (BCC), and face-centered cubic (FCC) Bravais lattices (see Fig. 1). We employ FEM to calculate the band structures and sound attenuation due to the complex geometry and the advantage of fast convergence of FEM. The dependence of band gaps on volume fraction of these triply periodic co-continuous structures is also discussed. We find large complete band gaps at sonic level existed in these structures, which may be the potential candidates for noise control.

## II. MATERIAL AND METHOD

Three types co-continuous structures with cubic symmetry are considered based on the level set structures of triply periodic minimal surfaces. A level surface is defined by a function of the form $F$: $\mathbf{R}^3 \rightarrow \mathbf{R}$ that satisfies the equation $F(x, y, z) = t$, where $t \in \mathbf{R}$ is a constant and $\{x, y, z\} \in \mathbf{R}^3$ are the coordinates of a point on the level surface. The level-set technique can be utilized to rapidly find suitable candidate functions that are invariant under the space group symmetry operations. The surface structures in Fig. 1 can be described by equations,[28]

$$\begin{aligned} f_{SC}(x,y,z) &= \cos(x)+\cos(y)+\cos(z)-0.5\cos(x)\cos(y) \\ &\quad -0.5\cos(y)\cos(z)-0.5\cos(z)\cos(x)+t, \\ f_{BCC}(x,y,z) &= \cos(x)\cos(y)+\cos(y)\cos(z)+\cos(z)\cos(x)+t, \\ f_{FCC}(x,y,z) &= 4\cos(x)\cos(y)\cos(z)+\cos(2x)\cos(2y) \\ &\quad +\cos(2y)\cos(2z)+\cos(2z)\cos(2x)+t, \end{aligned} \tag{1}$$

where $t$ is a constant that determines the volume fraction of the solid phase. As a result, the symmetry and volume distribution in these structures can be precisely controlled. Since the elastic impedance of the solid phase is larger than that of air, the wave propagating in air will be reflected by solid, and hence the propagation is predominant only in air. Therefore, the band structure calculation simplifies because the transverse speed of sound is zero in air.

The FEM software, COMSOL Multiphysics, is employed to calculate the band structure and sound attenuation. The governing equation of acoustic wave is the frequency-domain Helmholtz equation,

$$\nabla \cdot \left(\frac{-1}{\rho}\nabla p\right) + \frac{\omega^2 p}{\rho c_l^2} = 0, \tag{2}$$

where $p$ is the pressure, $\rho$ is the mass density, $\omega$ is the angular frequency, and $c_l$ is the speed of sound.

We assume that the triply periodic co-continuous structures are infinite and periodic in x, y, and z directions. The simulation is conducted on a unit cell to capture the infinite periodic nature of each structure through the Floquet periodicity boundary condition.[32] The unit cell is discretized using 10-node tetrahedron elements. The Floquet periodic condition is applied on the unit cell along three directions, respectively, and can be expressed as

$$\begin{aligned} p(x+a_1,y,z) &= p(x,y,z)\exp(ik_1a_1) \\ p(x,y+a_2,z) &= p(x,y,z)\exp(ik_2a_2) \\ p(x,y,z+a_3) &= p(x,y,z)\exp(ik_3a_3), \end{aligned} \tag{3}$$

where $a_1$, $a_2$, and $a_3$ are lattice constant and $(k_1, k_2, k_3)$ is the Bloch wave vector.[13]

The governing equation (2) combining with the boundary condition, Eq. (3), leads to the eigenvalue problem,

$$(\mathbf{K} - \omega^2\mathbf{M})p = 0, \tag{4}$$

where $\mathbf{K}$ and $\mathbf{M}$ are assembled matrix from the first and second term of Eq. (2), respectively. By scanning of $(k_1, k_2, k_3)$ in the first irreducible Brillouin zone, we obtain the corresponding eigenfrequencies and eigenmodes and hence the band structure can be constructed.

The sound attenuation is also calculated by the time-harmonic analysis of acoustic modulus. We stack seven unit cells along a specific direction in the first irreducible Brillouin zone to build the model. Sound hard boundary is applied on four lateral sides and a plane wave with pressure $p_0 = 1$ Pa incidents on the left boundary. The sound hard boundary can be given as

$$-\mathbf{n} \cdot \left(-\frac{1}{\rho_c}(\nabla p_t - q_d)\right) = 0, \tag{5}$$

where $\mathbf{n}$ is the normal vector, $\rho_c$ is the density of air, $p_t$ is pressure, and $q_d$ is Dipole source and the default value is zero.

The sound attenuation $d_w$ is defined as

$$\begin{aligned} d_w &= 10\log_{10}\left(\frac{w_{out}}{w_{in}}\right), \\ w_{out} &= \int_{\partial\Omega} \frac{|p|^2}{2\rho c_l}, \\ w_{in} &= \int_{\partial\Omega} \frac{|p_0|^2}{2\rho c_l}, \end{aligned} \tag{6}$$

where $w_{in}$ and $w_{out}$ denote incoming power at the inlet and the outgoing power at the outlet, respectively. $p_0$ and p are the pressure at the inlet and outlet, respectively.

Here PMMA is used as the solid phase, the material properties of which are given as follows: $\rho_{PMMA} = 1160\,kg/m^3$, $c_{PMMA} = 2700\,m/s$. The density and the sound speed of air are $\rho_{air} = 1.2\,kg/m^3$, $c_{air} = 343\,m/s$, respectively. The lattice constant is $a_1 = a_2 = a_3 = 2\,cm$ for all three types of co-continuous structures.

## III. RESULT AND ANALYSIS

### A. SC

#### 1. Band structure and transmission calculation

Fig. 2 illustrates the band structure and sound attenuation along ΓX direction of the triply periodic co-continuous structure with simple cubic lattice at volume fraction of 0.59. We find band gaps along specific direction. By overlapping these partial band gaps, we observed two complete band gaps in the band structure. The size of a band gap is usually expressed as the ratio of the gap width and the midgap frequency. As seen from Fig. 2, the lower CBG (between 9.002 kHz and 12.017 kHz) with the width of 0.287 appears between the first and second bands and the upper CBG (between 16.216 kHz and 17.101 kHz) with the width 0.053 lies between the fourth and fifth bands.

To verify the band structure calculation, the sound attenuation along ΓX direction is calculated by stacking seven unit cells along ΓX direction. The dips in sound attenuation figure agree well with the band gaps along ΓX direction, which indicates the calculated band structure is valid. The sound attenuation along other directions in the first irreducible Brillouin zone can also be calculated by stacking unit cells along the specific direction, which is not shown here.

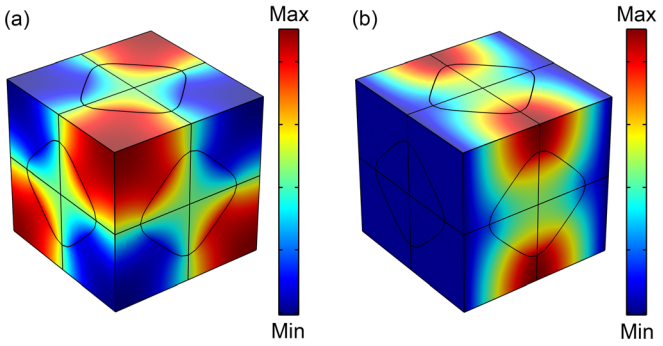


FIG. 3. The eigenmodes at (a) frequency = 9.002 kHz along ΓR direction and (b) frequency = 12.017 kHz along ΓX direction. The color scale denotes the amplitude of the pressure field.

#### 2. Acoustic modes

Fig. 3 shows the first and second eigenmodes at the R and X, respectively. The frequencies at R and X are 9.002 kHz and 12.017 kHz, respectively. The pressure field patterns of the above eigenmodes are observed to be symmetric with

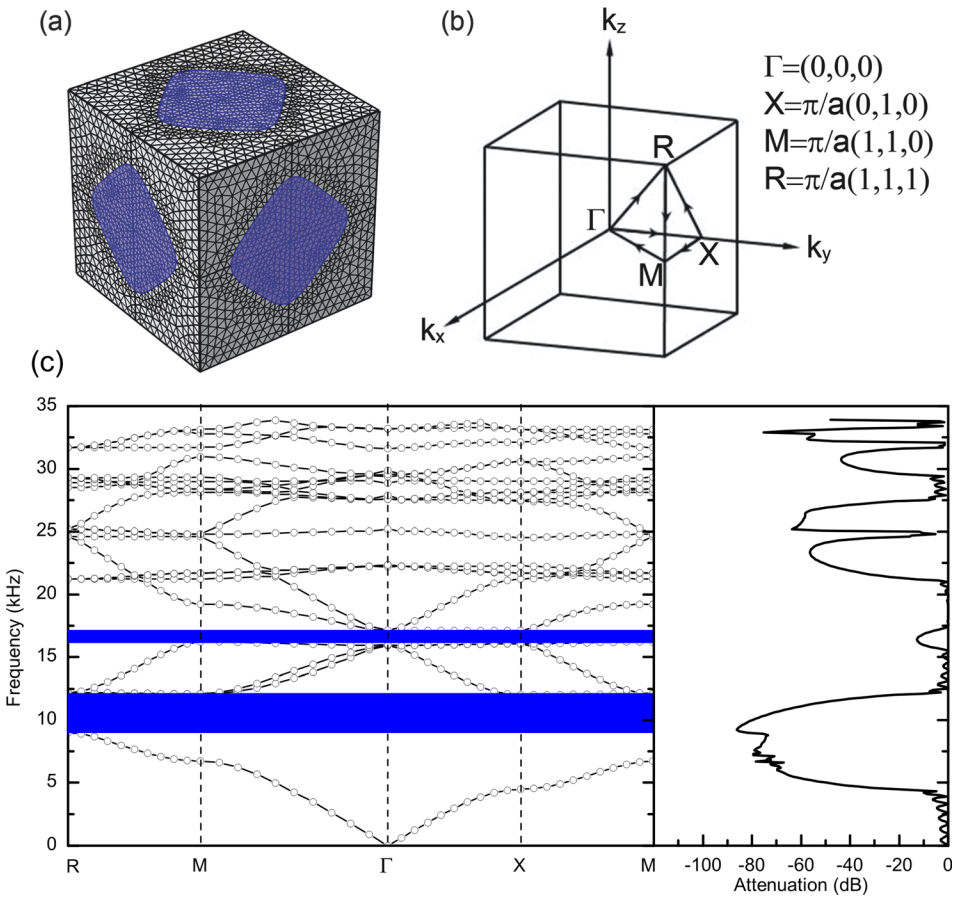


FIG. 2. (a) The unit cell of simple cubic lattice in FEM (The region in purple is PMMA), (b) the first irreducible Brillouin zone of simple cubic lattice, and (c) the band structure and sound attenuation along ΓX direction at the volume fraction of 0.59.

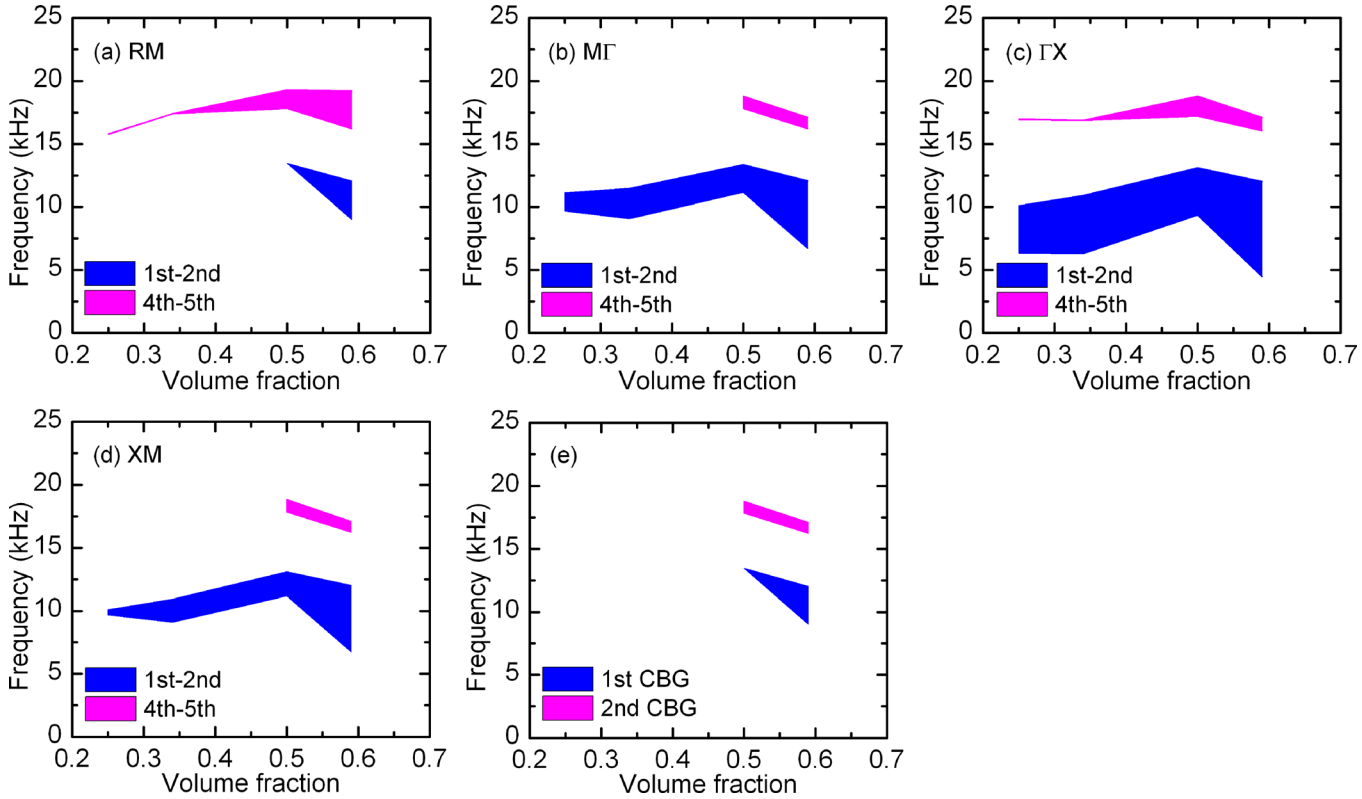


FIG. 4. (a)-(d) the band gap distribution as a function of solid volume fraction along RM, MΓ, ΓX, and XM, respectively, and (e) complete band gaps distribution.

respect to the plane ΓMR and plane ΓMX in the first irreducible Brillouin zone (see Fig. 2(b)), respectively.

#### 3. Effect of volume fraction on band gaps

The dependence of band gaps on volume fraction along different directions in the first irreducible Brillouin zone is also studied. Here we confine the volume fraction of PMMA between 0.20 and 0.70, within which the structure is reasonable from the perspective of multifunctionality. Since the CBGs appear between the first and second bands as well as the fourth and fifth bands, for comparative study we choose the band gaps along specific directions between these bands to study how the volume fraction variations affect the width of band gaps. Figs. 4(a)–4(d) show band gaps variations along RM, MΓ, ΓX, and XM, respectively. For the RM direction, we find the first band gap appears between the fourth and fifth bands, and the width of the band gaps widen as the volume fraction increases, while the band gaps between the first and second bands do not appear until the volume fraction reaches at 0.5. For the MΓ and XM direction, the first band gap appears between the first and second bands and the width of the band gaps almost keep constant till the volume fraction reaches at 0.5. For ΓX direction, we observe two band gaps appear at the same volume fraction and the lower one is much wider than the upper one. By overlapping the band gaps along the four directions, we find one CBG with the width of 0.053 at the volume fraction of 0.5 and two CBGs with the width of 0.287 and 0.053 at the volume fraction of 0.59. For the simple cubic lattice structure, the CBG appears until the volume fraction reaches 0.5.

### B. BCC

#### 1. Band structure and transmission calculation

Fig. 5 shows the band structure and sound attenuation along ΓH direction of the co-continuous structure with body-centered cubic lattice at the volume fraction of 0.52. There are three complete band gaps appearing in the band structure, which lie between first and second bands (between 6.462 kHz and 6.500 kHz), second and third bands (between 9.972 kHz and 14.398 kHz) and eighth and ninth bands (18.829 kHz and 21.224 kHz) with the width of 0.006, 0.363, and 0.120, respectively. Good agreement between sound attenuation and band structure along ΓH direction is also observed as shown in Fig. 5(c).

#### 2. Acoustic modes

Fig. 6 shows the second and third eigenmodes at the H and N, respectively. The frequencies at R and X are 9.972 kHz and 14.398 kHz, respectively. It is observed that the pressure field pattern of the eigenmodes at H and N are symmetric and antisymmetric with respect to the plane ΓNH and plane ΓNP in the first irreducible Brillouin zone (see Fig. 5(b)), respectively.

#### 3. Effect of volume fraction on band gaps

The dependence of band gaps on volume fraction along the four directions in the first irreducible Brillouin zone of BCC structure is illustrated in Figs. 7(a)–7(d). These band gaps lie between the bands where the complete band gaps

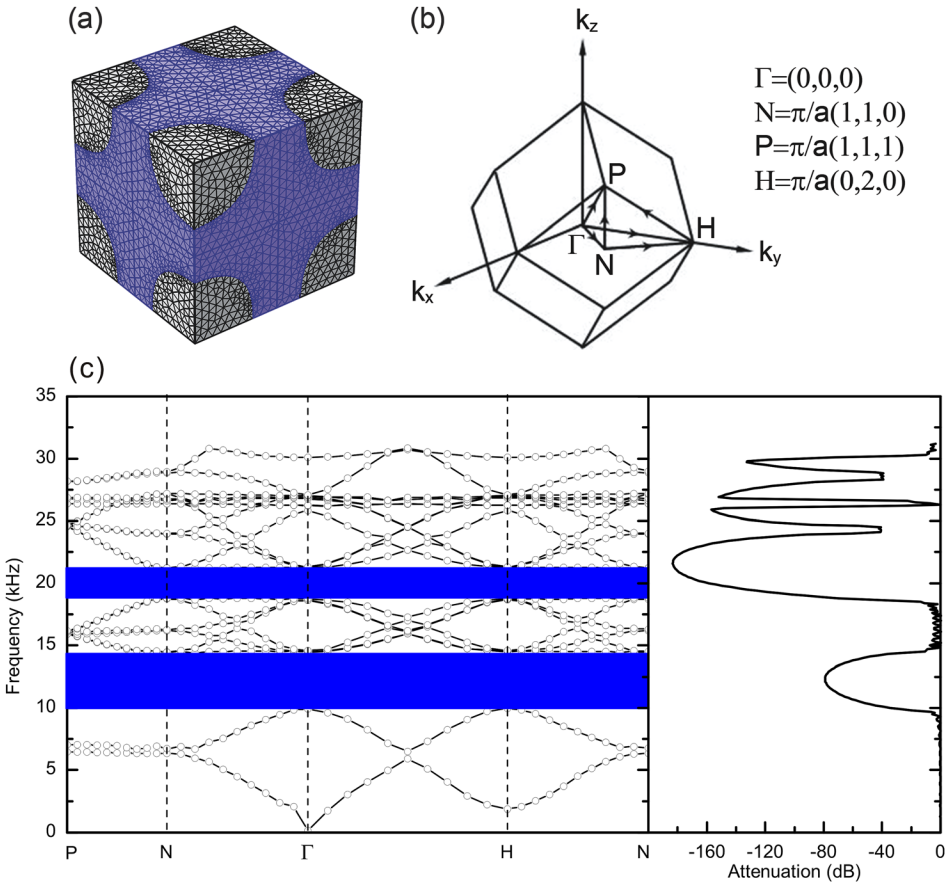


FIG. 5. (a) The unit cell of body-centered cubic lattice in FEM, (b) the first irreducible Brillouin zone of body-centered cubic lattice, and (c) the band structure and sound attenuation along ΓH direction at the volume fraction of 0.52.

appear. For the PN direction, three band gaps appear at the volume fraction range of 0.2 to 0.7, although the first and the third band gaps is relatively narrower compared with the second one. The width of the second band gaps increase when the volume fraction increases from 0.23 to 0.52 and keeps constant when the volume fraction lies between 0.52 and 0.59. The band gaps distribution along NΓ and HN are nearly the same, which is caused by the symmetry of the two directions in the first irreducible Brillouin zone. The second band gap are relatively larger than the first and third one, however, the second band gap does not appear until the volume fraction reaches at 0.52. For the ΓH direction, there are also three band gaps appears at the each volume fraction and the width of the second and the third band gaps can be neglected when the volume fraction below 0.35. The width of the second band gaps increases rapidly when the volume fraction is over 0.35, which means that the volume fraction has a great impact on the width. Fig. 7(e) is the complete band gaps distribution at different volume fraction, which is also constructed by overlapping the band gaps along the four directions. Fortunately, we find three complete band gaps when the volume fraction at 0.52–0.59, the largest width of which are 0.436, 0.539, and 0.238, respectively. Compared with SC structures, the number and the width of complete band gaps of BCC structures are both larger than those of SC structures.

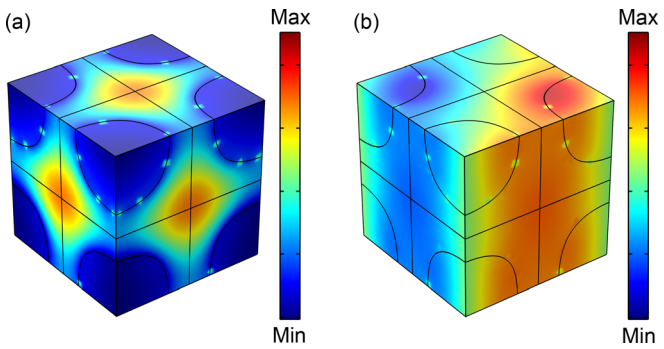


FIG. 6. The eigenmodes at (a) frequency = 9.972 kHz along ΓH direction and (b) frequency = 14.398 kHz along ΓN direction. The color scale denotes the amplitude of the pressure field.

## C. FCC

### 1. Band structure and transmission calculation

The band structure and sound attenuation along ΓX direction of the co-continuous structure with face-centered cubic lattice at the volume fraction of 0.54 are also calculated, as show in Fig. 8. We find two complete band gaps in the band structure, which lie between the fourth and the fifth bands (between 10.803 kHz and 18.076 kHz) and sixteenth and seventeenth bands (24.589 kHz and 26.929 kHz) with the width of 0.504 and 0.091, respectively. The sound attenuation also matches the band structure along ΓX direction very well as seen in Fig. 8(c).

### 2. Acoustic modes

Fig. 9 shows the fourth and fifth eigenmodes at the X and L, respectively. The frequencies at X and L are

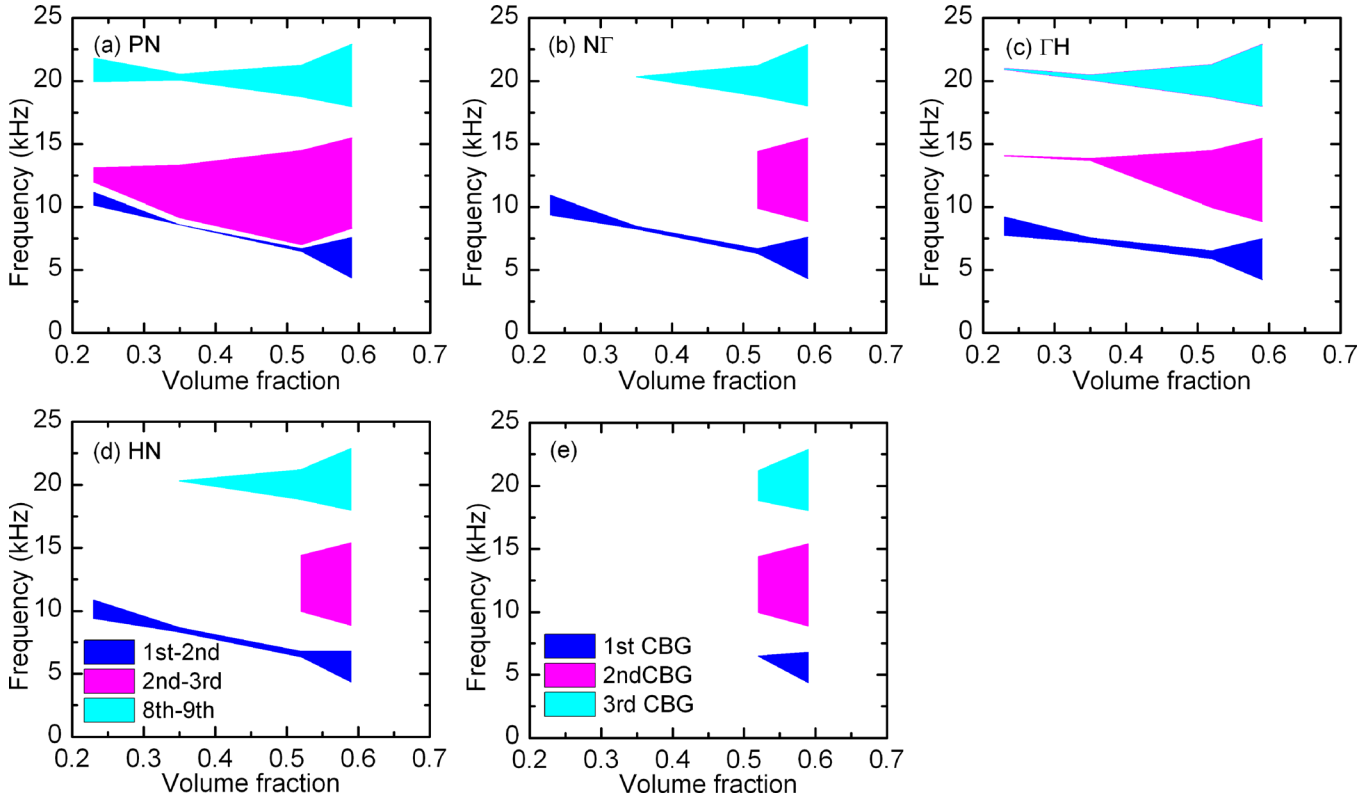


FIG. 7. (a)–(d) the band gap distribution as a function of solid volume fraction along PN, NΓ, ΓH, and HN, respectively, and (e) complete band gaps distribution.

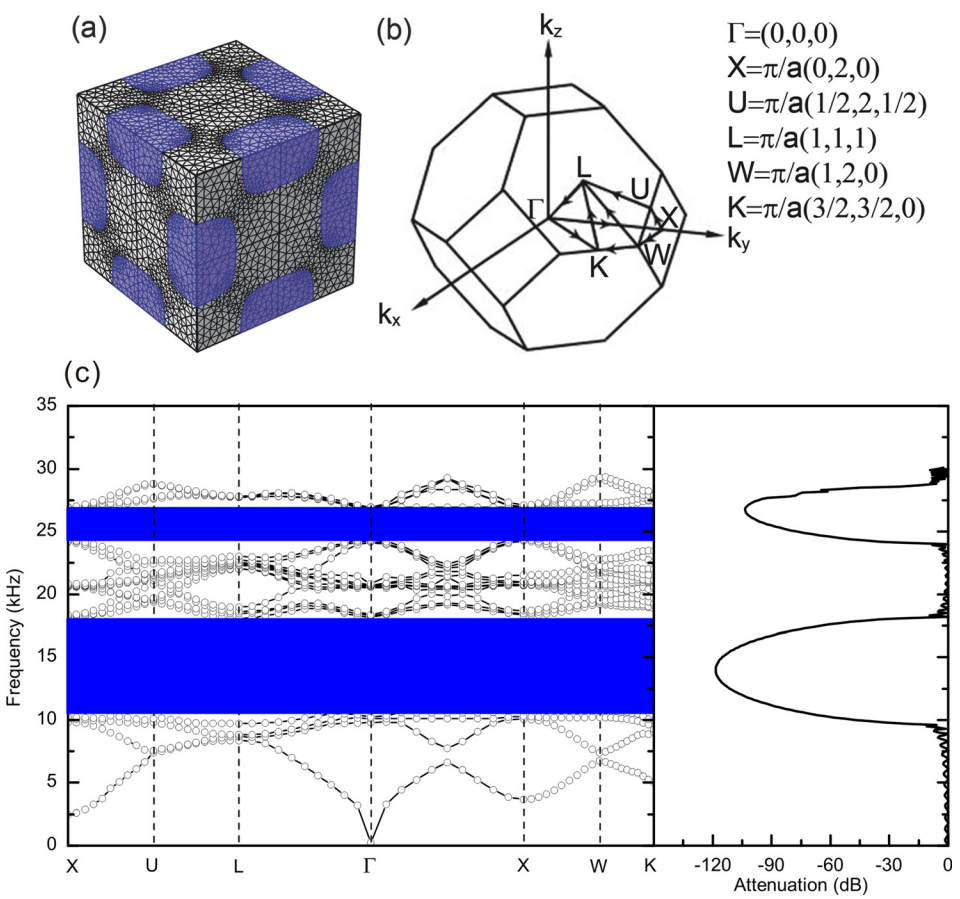


FIG. 8. (a) The unit cell of face-centered cubic lattice in FEM, (b) the first irreducible Brillouin zone of face-centered cubic lattice and (c) the band structure and sound attenuation along ΓX at the volume fraction of 0.54.

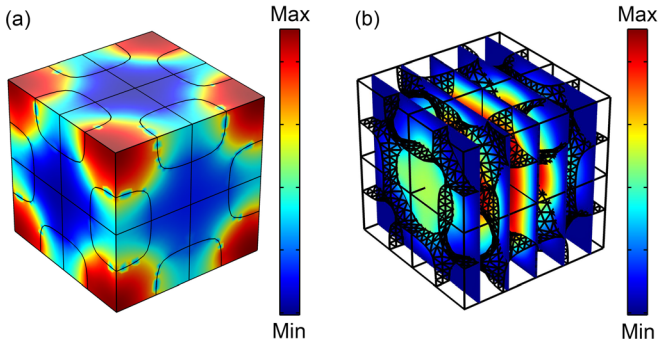


FIG. 9. The eigenmodes of (a) frequency = 10.803 kHz along ΓX direction and (b) frequency = 18.076 kHz along ΓL direction. The color scale denotes the amplitude of the pressure field.

10.803 kHz and 18.076 kHz, respectively. It is shown that the pressure field pattern of the eigenmodes at X is symmetric with respect to the plane GKWX in the first irreducible Brillouin zone in Fig. 8(b). The surface pressure field pattern of the eigenmodes at L is nearly uniform. However, we observe that the total pressure field pattern of the eigenmodes at L is also symmetric with respect to the plane GKWX when we take slices from the unit cell, which is shown in Fig. 9(b).

### 3. Effect of volume fraction on band gaps

Figs. 10(a)–10(f) show the band gaps distribution along the six directions in the first irreducible Brillouin zone of FCC structure. We observe three band gaps along the six directions and the width of the first one lying between third and fourth bands is relatively smaller compared with the other two gaps. The second ban gap is the largest among three of them at the same volume fraction and enlarges rapidly when the volume fraction increases from 0.25 to 0.62.

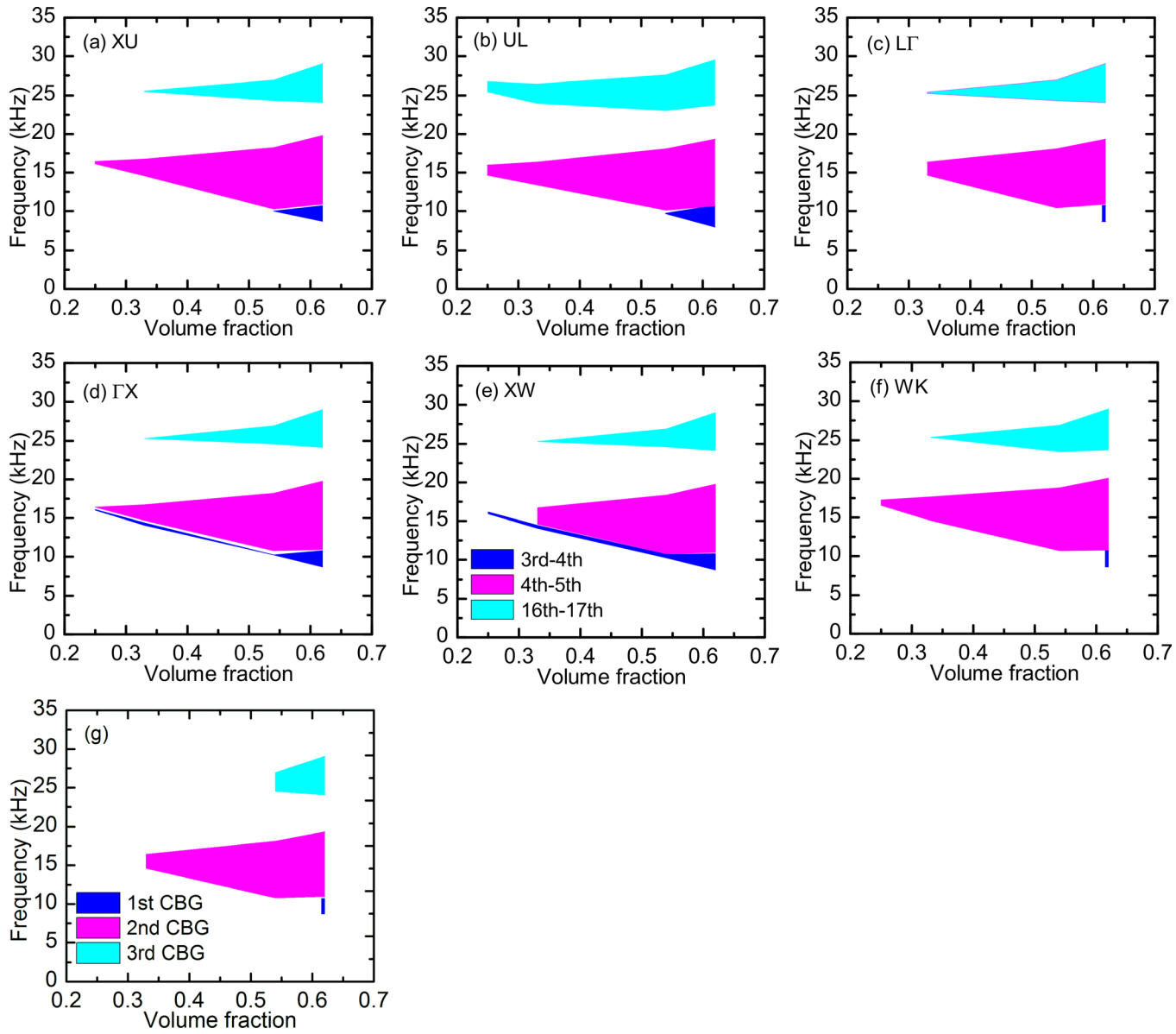


FIG. 10. (a)–(f) the band gap distribution as a function of solid volume fraction along XU, UL, LΓ, ΓX, XW, and WK, respectively, and (g) complete band gaps distribution.

The third band gap opens at the volume of 0.33 along the six directions expect the UL direction and then become wider when the volume fraction is increased. Fig. 10(g) shows the complete band gaps distribution at different volume fraction, which is also constructed by overlapping the band gaps along the four directions. We also find three complete band gaps, the largest width of which are 0.205, 0.548, and 0.185, respectively. Although the width of largest complete band gap of BCC structures and FCC structures are nearly the same, the second band gap of FCC structure opens at the volume fraction of 0.33, which is much lower than that of BCC structures. Therefore, FCC structures are more favorable for the opening of complete band gap compared with SC and BCC structures.

## IV. CONCLUSION

In summary, we have investigated the acoustic band structure and sound attenuation of three types of triply periodic co-continuous structures with SC, BCC and FCC lattices, respectively. Good agreement between band gaps and dips of sound attenuation is achieved. Complete band gaps for the three types co-continuous structures are observed at the volume fraction from 0.2–0.7. The largest band gap width of BCC and FCC structures is nearly twice than that of SC structures. FCC structures are more favorable for formation of CBGs than other two structures since the complete band gaps open at much lower volume fraction. Compared with other studies on acoustic band gaps of three-dimensional structures, the band gaps width of BCC and FCC structures are much wider.[15,23] In addition, all of the largest complete band gaps lie in the audible range of frequencies (0–20 kHz) and cover half range of it, which indicates that these structures can be applied to control noise. It should note that these triply periodic co-continuous structures can be easily fabricated by 3D direct-write printing.

Here, we do not consider the effect of deformation induced by acoustic wave and structure interaction on the width of band gaps. However, the width of band gap of phononic crystals can be tuned by mechanically trigged large deformation as well as the shape-memory effect.[33–35] Future studies include experimental investigation on sound attenuation/transmission of the studied composite structures and furthermore, the elastic wave propagation properties in these composites with different material combinations and the effect of deformation on the evolution of band gaps will be explored.

## ACKNOWLEDGMENTS

This work was partially supported by the National Science Foundation under Award number CMMI-1234768. The authors thank Professor Katia Bertoldi (Harvard University) for helpful discussions.

[1]A. Khelif, A. Choujaa, B. Djafari-Rouhani, M. Wilm, S. Ballandras, and V. Laude, Phys. Rev. B **68**, 214301 (2003).
[2]M. S. Kushwaha, Appl. Phys. Lett. **70**, 3218 (1997).
[3]M. Sigalas, J. Appl. Phys. **84**, 3026 (1998).
[4]R. Weaver, Wave Motion **12**, 129–142 (1990).
[5]S. S. Lin and T. J. Huang, J. Appl. Phys. **106**, 053529 (2009).
[6]D. Yu, J. Wen, H. Zhao, Y. Liu, and X. Wen, J. Sound Vib. **318**, 193–205 (2008).
[7]J. Lee, L. Wang, S. Kooi, M. C. Boyce, and E. L. Thomas, Nano Lett. **10**, 2592 (2010).
[8]J. Lee, J. P. Singer, and E. L. Thomas, Adv. Mater. **24**, 4782–4810 (2012).
[9]F. Meseguer, M. Holgado, D. Caballero, N. Benaches, C. Lopez, J. Sanchez-Dehesa, and J. Llinares, J. Lightwave Technol. **17**, 2196 (1999).
[10]L. Dhar and J. A. Rogers, Appl. Phys. Lett. **77**, 1402 (2000).
[11]P. McIver, Appl. Ocean Res. **24**, 121 (2002).
[12]M. Alam, Phys. Rev. Lett. **108**, 084502 (2012).
[13]M. Kushwaha, P. Halevi, L. Dobrzynski, and B. Djafari-Rouhani, Phys. Rev. Lett. **71**, 2022 (1993).
[14]M. Kushwaha, P. Halevi, G. Martinez, L. Dobrzynski, and B. Djafari-Rouhani, Phys. Rev. B **49**, 2313 (1994).
[15]M. Kushwaha and B. Djafari-Rouhani, J. Appl. Phys. **80**, 3191 (1996).
[16]M. Kushwaha and P. Halevi, J. Acoust. Soc. Am. **101**, 619 (1997).
[17]E. Economou and M. Sigalas, J. Acoust. Soc. Am. **95**, 1734–1740 (1994).
[18]D. Garcia-Pablos, M. Sigalas, F. Montero de Espinosa, M. Torres, M. Kafesaki, and N. Garcia, Phys. Rev. Lett. **84**, 4349 (2000).
[19]C. Goffaux and J. Vigneron, Phys. Rev. B **64**, 075118 (2001).
[20]J. Vasseur, P. Deymier, B. Chenni, B. Djafari-Rouhani, L. Dobrzynski, and D. Prevost, Phys. Rev. Lett. **86**, 3012 (2001).
[21]F. Montero de Espinosa, E. Jiménez, and M. Torres, Phys. Rev. Lett. **80**, 1208 (1998).
[22]Z. Y. Cui, T. N. Chen, J. H. Wu, H. L. Chen, and B. Zhang, Appl. Phys. Lett. **93**, 144103 (2008).
[23]L. Wu and L. Chen, J. Phys. D **44**, 045402 (2011).
[24]M. Sigalas, M. S. Kushwaha, E. N. Economou, M. Kafesaki, I. E. Psarobas, and W. Steurer, Z. Kristallogr. **220**, 765 (2005).
[25]E. L. Thomas, D. M. Anderson, C. S. Henkee, and D. Hoffman, Nature **334**, 598 (1988).
[26]Y. Lu, Y. Yang, A. Sellinger, M. Lu, J. Huang, H. Fan, R. Haddad, G. Lopez, A. R. Burns, and D. Y. Sasaki, Nature **410**, 913 (2001).
[27]Y. Ha, R. A. Vaia, W. F. Lynn, J. P. Costantino, J. Shin, A. B. Smith, P. T. Matsudaira, and E. L. Thomas, Adv. Mater. **16**, 1091–1094 (2004).
[28]M. Maldovan, C. K. Ullal, J. Jang, and E. L. Thomas, Adv. Mater. **19**, 3809 (2007).
[29]S. Torquato, S. Hyun, and A. Donev, Phys. Rev. Lett. **89**, 266601 (2002).
[30]S. Torquato and A. Donev, Proc. R. Soc. London A **460**, 1849 (2004).
[31]L. F. Wang, J. Lau, E. L. Thomas, and M. C. Boyce, Adv. Mater. **23**, 1524 (2011).
[32]S. Barone, M. Narcowich, and F. Narcowich, Phys. Rev. A **15**, 1109 (1977).
[33]K. Bertoldi and M. Boyce, Phys. Rev. B **78**, 184107 (2008).
[34]L. F. Wang and K. Bertoldi, Int. J. Solid. Struct. **49**, 2881 (2012).
[35]J. Jang, C. Y. Koh, K. Bertoldi, M. C. Boyce, and E. L. Thomas, Nano Lett. **9**, 2113–2119 (2009).